Astronomy & Astrophysics manuscript no.
(will be inserted by hand later)

Dust trapping in thin-ringed protoplanetary disks

C.P. Dullemond[1], T. Birnstiel[2], L. Perez[3], S. Andrews[4], A. Isella[5], J. Huang[4], Z. Zhu[6], V. Guzmán[7], M. Benisty[8], J. Carpenter[9]

(1) Zentrum für Astronomie, Heidelberg University, Albert Ueberle Str. 2, 69120 Heidelberg, Germany
(2) **XXXX** (3) **XXXX** (4) **XXXX** (5) **XXXX** (6) **XXXX**

May 16, 2018

Abstract. A large fraction of the protoplanetary disks observed with the ALMA Large Programme **XXXX** display multiple well-defined and nearly perfectly circular rings in the continuum, in many cases with substantial peak-to-valley contrast. Several of these rings are very narrow in radial extent. In this paper we analyze these results using the assumption that these dust rings are caused by dust trapping in radial pressure bumps. We model this process in a 1-D axisymmetric way, initially with a simple analytic model, then with a more detailed numerical model. We find that ..... **CONCLUSIONS**

Key words. accretion, accretion disks – circumstellar matter – stars: formation, pre-main-sequence – infrared: stars

1. Introduction

The concept of dust trapping in local pressure maxima has become a central theme in studies of planet formation and protoplanetary disk evolution, as it may provide an elegant solution to several problems in these fields of study. Theories of planet formation are plagued by the "radial drift barrier": the problem that as dust aggregates grow by coagulation, they tend to radially drift toward the star before they reach planetsimal size (e.g. Birnstiel et al. 2010). A natural solution to this problem could be the trapping of dust particles in local pressure maxima (Whipple 1972; Kretke & Lin 2007; Barge & Sommeria 1995; Klahr & Henning 1997). From an observational perspective, the radial drift problem manifests itself by the presence of large grains in the outer regions of protoplanetary disks (Testi et al. 2003; Andrews et al. 2009), which appears to be in conflict with theoretical predictions (Brauer et al. 2007). One possible solution to this observational conundrum could be that the disks are much more massive in the gas than previously suspected, leading to a higher gas friction for millimeter grains and thus longer drift times (Powell et al. 2017). But another explanation is to invoke, again, pressure traps. The most striking observational evidence for dust trapping seems to come from large transitional disks, which feature giant dust rings, sometimes lopsided, in which large quantities of dust appears to be concentrated (Casassus et al. 2013; van der Marel et al. 2013). These observations appear to be well explained by the dust trapping scenario Pinilla et al. (2012a). But these transitional disks seem to be rather violent environments, possibly with strong warps (Marino et al. 2015; Benisty et al. 2017) and companion-induced spirals (Dong et al. 2016). For more "normal" protoplanetary disk the dust traps would have to be more subtle. Pinilla et al. (2012b) explored the possibility that the disk features many axisymmetric local pressure maxima, and calculated how the dust drift and growth would behave under such conditions. It was found that, if the pressure bumps are strong enough, the dust trapping can keep a sufficient fraction of the dust mass at large distances from the star to explain the observed dust millimeter flux. It would leave, however, a detectable pattern of rings that should be discernable with ALMA observations. Since the multi-ringed disk observation of HL Tau (ALMA Partnership et al. 2015) a number of such multi-ringed disks have been detected (Andrews et al. 2016; Isella et al. 2016; Cieza et al. 2017; Fedele et al. 2017, 2018). It is therefore very tempting to see also these multi-ringed disks as evidence for dust trapping, and as an explanation for the retention of dust in the outer regions of protoplanetary disks.

The data from the ALMA Large Programme 2016.1.00484.L offers an exciting new opportunity to put this concept to the test, and to put constraints on the physics of dust trapping in axisymmetric pressure maxima. This is an opportunity which we explore in this paper.

If we assume that the rings seen in our data are caused by dust trapping, the question arises: what constraints do the data impose on the physics of dust trapping? To explore this we start by studying the rings individually, assuming that the dust does not escape from the ring. This makes it possible to look for a steady-state dust trapping model in which the radial drift forces (that push the dust

to the pressure peak) are balanced by turbulent mixing (that tends to smear out the dust away from the pressure peak). In Section 3 we will construct a very simplified analytic dust trapping model, and confront this with the most well-isolated rings from our sample. **Describe the next sections.** But before we do the modeling, we review, in Section 2, the key aspects of the data from our ALMA Large Programme that we compare our models to.

2. The high-contrast rings of AS 209, Elias 24, GW Lup, HD 143006 and HD 163296

In this paper we discuss in particular those sources of the ALMA Large Programme that show high-contrast and radially thin rings that are separated by deep valleys, and that are sufficiently face-on to not have to worry about 3-D lie-of-sight aspects. These are AS 209, Elias 24, GW Lup, HD 143006 and HD 163296. The high-contrast rings of these sources provide "clean laboratories" for testing the theory of dust trapping, both in a ring-by-ring manner, as well as by comparing to global dust drift models. The most striking case is AS 209, which features two high-contrast radially thin rings which are isolated and large (**see Guzmán et al. (2018) for the detailed description of this dataset**). Fig.1 shows the radial profile (deprojected for inclination) of the thermal emission of the dust of the disk around AS 209. The brightness is expressed as linear brightness temperature ($T_{\rm bright,linear} = (c^2/2k_B)I_\nu/\nu^2$), where I_ν is the intensity, c the light speed, k_B the Boltzmann constant, and ν the frequency. It should be noted that the full (non-linear) brightness temperature (defined such that $B_\nu(T_{\rm bright,full}) = I_\nu$, with $B_\nu(T)$ the Planck function) can have very different values, in particular at low brightness. As a result $T_{\rm bright,full}(r)$ tends to vastly underestimate the contrast between the rings and the inter-ring regions. Therefore, in this paper we plot the brightness using the linear brightness temperature.

The two most prominent rings (seen as bumps in Fig.1) are fitted by Gaussian profiles with a standard deviation width of 4.0 au and 4.4 au respectively. This corresponds to a full-width-at-half-maximum (FWHM) of 9.3 au and 10.3 au. The ALMA beam FWHM for these observations is roughly 4.4 au, meaning that the rings are 2.1 and 2.3 beams wide.

These Gaussian profiles fit the observed data remarkably well, even in the wings of the profile (except the outer wing of the outer ring). This is somewhat surprising, given that the rings are resolved. The Gauss profiles therefore do not represent the beam profile, but tell something about the actual dust distribution within the ring.

The source Elias 24 also shows a prominent high-contrast isolated ring, albeit flanked on the outside by a plateau of emission (see **Andrews et al. (2018) for a detailed description of this dataset**).

The ring can be reasonably well fitted with a Gaussian profile with standard deviation width of 5.0 au corresponding to a FWHM of 11.7 au. Given a beam size in band 6 of about 4.9 au, the ring of Elias 24 is also resolved by about 2.4 beam widths. The Gaussian fit is, however, less convincing in the case of Elias 24 than in the case of AS 209, so that it cannot be clearly argued that the ring has a Gaussian shape in the case of Elias 24.

[TODO: GW Lup, HD 143006 and HD 163296]

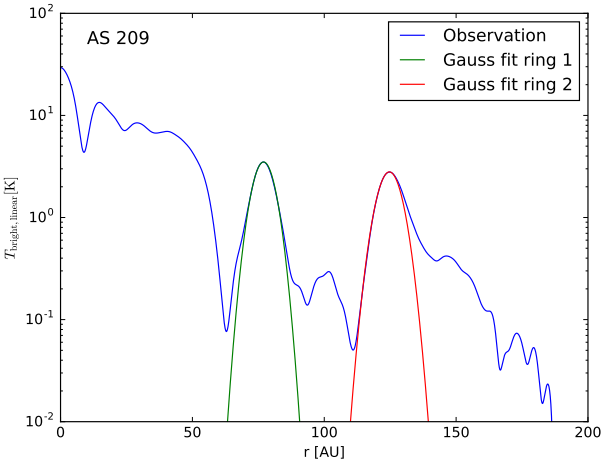

Fig. 1. The linear brightness temperature in band 6 of the disk around AS 209, as a function of deprojected distance to the star (see **Guzmán et al. (2018)** for a detailed description and analysis of these data). The vertical axis is logarithmic to better show the contrast. The two most prominent rings are fitted by Gaussian rings. Ring 1 is fitted by $T_{\rm bright,linear}(r) = 3.5\,\exp(-0.5(r - 77\,{\rm au})^2/(4.0\,{\rm au})^2)$, while ring 2 is fitted by $T_{\rm bright,linear}(r) = 2.8\,\exp(-0.5(r - 124.7\,{\rm au})^2/(4.4\,{\rm au})^2)$.

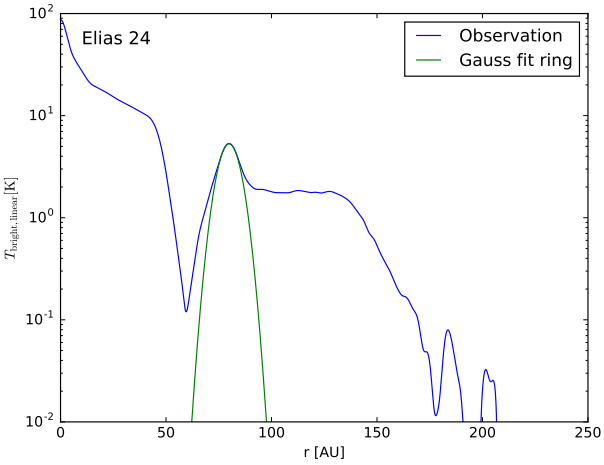

Fig. 2. As Fig. 1, but now for the source Elias 24 (see **Andrews et al. (2018)** for a detailed description and analysis of these data). The most prominent ring is fitted by a Gaussian profile $T_{\rm bright,linear}(r) = 5.3\,\exp(-0.5(r - 79.9\,{\rm au})^2/(5.0\,{\rm au})^2)$.

3. Steady-state dust distribution in a ringlike trap

Given the nicely separated narrow rings in the above sources, we can analyze these rings on a one-by-one basis. This is what we will do in this Section. We will assume that the dust trapping in these rings is absolute: no dust escapes. But increased turbulent mixing can spread the dust over a broader ring. Before we start constructing a model, we will discuss an important feature of the observed rings: that they appear to be radially resolved, Gaussian in shape, yet sub-Planckian in brightness. We will present a simple analytic dust trapping model, and show which radial brightness profiles it predicts, depending on the dust size distribution, the turbulent strength and the gas pressure bump width. This, when compared to the data, will allow us to draw some conclusions about the size distribution [**and perhaps more?**].

3.1. Resolved ring width and the brightness temperature

If our finding is correct that the rings in our sample are all spatially resolved in radial direction, then this poses an interesting question. In many cases the brightness of these rings is arguably sub-Planckian. This is, for instance, the case for the high-contrast rings of AS 209, as well as **XXXXXXX**. For the outer two rings of AS 209 (at 77 au and 125 au, respectively, the non-linear brightness temperatures are 3.5 K and 2.8 K, respectively. If these rings would have been *un*resolved, then this sub-Planckian emission is easily explained by the ring not filling the beam. But because these rings are radially resolved, this scenario should be rejected. The remaining possibilities are that the disk is colder than we think or that the rings are optically thin. In the latter case the spectral slope $\alpha_{\rm spec}$ at the location of these rings, once measured, will determine if the grains that are trapped in this ring are smaller, similar or larger than about $\lambda/2\pi$, where λ is the wavelength around which the slope is measured. If we use $\lambda = 0.13\,$cm and $\lambda = 0.31\,$cm (representing ALMA band 6 and 3, respectively) to determine $\alpha_{\rm spec}$ this would mean we can distinguish between grains smaller, similar or larger than about 300 μm. A low $\alpha_{\rm spec}$ would imply grains that are substantially larger than 300 μm, i.e. of the order of millimeter or larger.

In several recent observations of the spectral index across ringed disks (ALMA Partnership et al. 2015; Huang et al. 2018) one clearly sees that $\alpha_{\rm spec}$ varies across these rings, being closer to 2 at the ring center and substantially larger between the rings. This makes sense in terms of the dust trapping scenario in which we expect larger grains to be trapped more efficiently (and thus dominate the peak of the ring) than smaller grains, because the smaller grains will be more subject to turbulent mixing. This scenario requires a grain size distribution, so that the width of the dust ring is smaller for the bigger grains and bigger for the smaller ones.

While this scenario is plausible and appealing, one may worry that it requires some fine-tuning. Why would the rings be dominated by a population of grains that are larger than 300 μm, but not too large, for else they would be so effectively trapped that they would produce an even narrower ring? For one or two sources that could be coincidence, but for a multitude of sources this is less plausible. One possible explanation is that millimeter grains are indeed the largest grains in the outer regions protoplanetary disks, because larger grains would easily get destroyed and/or simply bounce instead of stick when they collide, and thus not grow further (Güttler et al. 2010; Zsom et al. 2010). These models also predict larger grains to drift quickly inward, but that is only valid for a model without dust traps. At any rate: perhaps millimeter grains are a natural consequence of dust growth. If so, it then remains to be understood why the combination of turbulent strength and gas surface density conspire to trap these millimeter grains, but not too much, for else we might expect at least some rings to be narrower than a pressure scale height. We are aware that, even with a sample of 20 sources, we are still in the small-number-statistics regime, so these considerations are limited in their strength.

In this section we will study this question using a very simple model of a dust trap: a parameterized gaussian pressure profile. The goal is to find out if the variations of $\alpha_{\rm spec}$ across the ring are naturally produced, while still keeping the dust ring radially resolved, without having to fine-tune the size distribution of the grains, the turbulence of the gas or other parameters. We will do this in several steps, starting with analytic solutions in Subsection **??**, and proceeding with DISKLAB models in Subsection **??**.

3.2. Analytic approximate solution of dust trapping

Let us consider a narrow gas ring around the star at radius r_0 with a midplane pressure given by

$$p(r) = p_0 \exp\left(-\frac{(r-r_0)^2}{2w^2}\right) \tag{1}$$

where $w \ll r_0$ is the parameter setting the width of this gaussian ring. We assume that the gas is weakly turbulent with turbulent diffusion coefficient D. Dust grains get trapped in this ring, and the dust will acquire a radial density profile that is in equilibrium between the radial dust drift pointing toward the peak of the gas pressure and radial turbulent diffusion pointing away from that position. The radial dust drift velocity is (see e.g.):

$$v_{\rm dr} = \frac{1}{\mathrm{St} + \mathrm{St}^{-1}} \left(\frac{d\ln p}{d\ln r}\right) \frac{c_s^2}{\Omega_K r} \tag{2}$$

where c_s is the isothermal sound speed and the Stokes number St is defined as

$$\mathrm{St} = \Omega_K t_{\rm stop} \tag{3}$$

where $t_{\rm stop}$ is the stopping time of the grains. The diffusion coefficient for the dust is (Youdin & Lithwick 2007):

$$D_{\rm d} = \frac{D}{1+\mathrm{St}^2} \tag{4}$$

We take D to be equal to the turbulent viscosity ν divided by the Schmidt number Sc, which we usually set to $\mathrm{Sc} = 1$. We use the usual α-prescription for the turbulence:

$$D = \frac{\nu}{\mathrm{Sc}} = \alpha_{\mathrm{turb}} \frac{c_s^2}{\mathrm{Sc}\,\Omega_K} \tag{5}$$

If D is sufficiently small, the dust will get concentrated into a ring with width w_d that is substantially smaller than the width of the gas ring w. Also the dust will all be settled vertically into a layer that has a vertical thickness less than the gas pressure scale height. In that case the solution to the drift-mixing equation for the dust becomes simple, because we can then assume everything to be constant with r (within this limited domain), except for the gas pressure gradient. We will also ignore any terms arising from the curvature of the coordinates. The steady-state radial dift-mixing equation for the dust then becomes, in its approximate form:

$$\frac{d}{dr}\left(\Sigma_{\mathrm{d}} v_{\mathrm{dr}} - D_{\mathrm{d}} \frac{d\Sigma_{\mathrm{d}}}{dr}\right) = 0 \tag{6}$$

Integrating this equation once, with integration constant zero (which amounts to a zero net radial flux), yields

$$\Sigma_{\mathrm{d}} v_{\mathrm{dr}} = D_{\mathrm{d}} \frac{d\Sigma_{\mathrm{d}}}{dr} \tag{7}$$

From Eqs.(2,1) we can express v_{dr} as

$$v_{\mathrm{dr}} = -\left(\frac{c_s^2}{w^2 \Omega_K (\mathrm{St} + \mathrm{St}^{-1})}\right)(r - r_0) \tag{8}$$

With this expression we can solve Eq. (7) for Σ_{d}:

$$\Sigma_{\mathrm{d}}(r) = \Sigma_{\mathrm{d0}} \exp\left(-\frac{(r-r_0)^2}{2w_{\mathrm{d}}^2}\right) \tag{9}$$

with

$$w_{\mathrm{d}} = w\sqrt{\frac{\Omega_K D_{\mathrm{d}} (\mathrm{St} + \mathrm{St}^{-1})}{c_s^2}} = w\sqrt{\frac{\alpha_{\mathrm{turb}}}{\mathrm{Sc}\,\mathrm{St}}} \tag{10}$$

Note that this is only valid as long as $\alpha_{\mathrm{turb}} \ll \mathrm{Sc}\,\mathrm{St}$. This solution is, in fact, the radial version of the vertical settling-mixing equilibrium solutions of Dubrulle et al. (1995).

Now let us introduce a grain size distribution. Since the trapping width w_{d} for the different grain sizes is different, we can only impose the grain size distribution for the total (radially integrated) dust mass. We define the size distribution according to the following powerlaw

$$m(a)\frac{dN}{d\ln a} = \frac{dM}{d\ln a} \propto a^q \tag{11}$$

where a is the grain size, $m(a)$ the corresponding grain mass, N the cumulative particle number and M the cumulative dust mass. The parameter q is the size distribution powerlaw coefficient, and it is $q = 1/2$ for the usual MRN distribution (this corresponds to $dN/da \propto a^{-3.5}$). We also need to define limits a_{min} and a_{max}. The size distribution is then normalized such that its integral over $d\ln(a)$ is the total dust mass M. The radial surface density solution, Eq. (9), then becomes:

$$\frac{d\Sigma_{\mathrm{d}}(r)}{d\ln a} = \frac{1}{(2\pi)^{3/2} r_0 w_{\mathrm{d}}(a)} \frac{dM}{d\ln a} \exp\left(-\frac{(r-r_0)^2}{2w_{\mathrm{d}}(a)^2}\right) \tag{12}$$

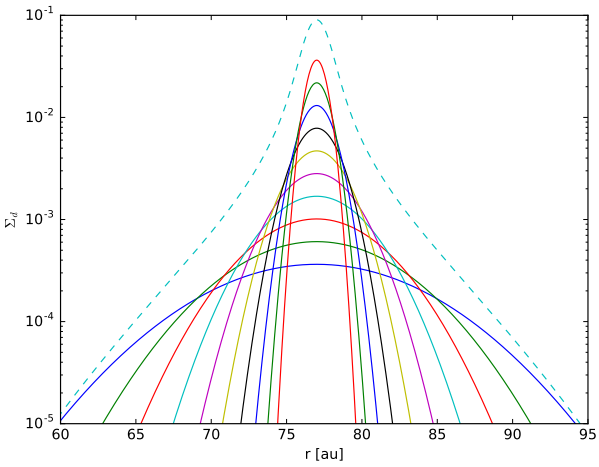

Fig. 3. Results of the analytic dust trapping model for an MRN powerlaw grain size distribution between $a = 0.01\,\mathrm{cm}$ and $a = 1\,\mathrm{cm}$. The gas pressure bump has a FWHM of 70 au and a peak at $r = 77\,\mathrm{au}$. Shown here are the surface density profiles for 10 logarithmically binned grain sizes. The curve with the narrowest peak corresponds to a grain size of $a = 1\,\mathrm{cm}$, while that with the widest peak (and lowest maximum value) corresponds to a grain size of $a = 0.01\,\mathrm{cm}$. The intermediate curves correspond to $a = 0.0167$, 0.0278, 0.0464, 0.0774, 0.1291, 0.2154, 0.3593 and 0.5995 cm respectively. The dashed curve shows the total surface density of the dust, which is, by definition of the bin-integrated surface density, the sum of all 10 curves. For a description of the model setup and model parameters, see Section 3.3.

3.3. Resulting profiles for a size distribution

The analytic model of the dust trapping for a single grain size speaks for itself. But how does it look for a grain size distribution? In Fig. 3 we show the radial profiles for an MRN size distribution between $a_{\mathrm{min}} = 10^{-2}\,\mathrm{cm}$ and $a_{\mathrm{min}} = 1\,\mathrm{cm}$ and a total dust mass of $M = 1.3 \times 10^{-5}\,M_\odot$. The dust material density is taken to be $\xi_{\mathrm{dust}} = 2\,\mathrm{g/cm^3}$. We sample this size distribution with 10 grain sizes, evenly distributed in $\ln(a)$. These are the 10 curves in Fig. 3. These surface densities are defined as being the local grain size distribution integrated over the width of the grain size bin: $\Sigma_{\mathrm{bin}} = \int_{\mathrm{bin}} (d\Sigma_{\mathrm{dust}}/da)da$. The stellar mass is $M_* = 0.9\,M_\odot$ and we set $\mathrm{Sc} = 1$.

MUST ALSO SPECIFY GAS DENSITY, TO GET STOKES NUMBERS. MUST SAY (AND CHECK) THAT EPSTEIN REGIME.

As expected, the largest grains are concentrated the most and the smallest ones the least. The largest grains, however, have the largest peak value of their surface density at the exact location of the gas pressure peak.

When it comes to the contribution to the optical depth, however, the situation looks a bit different. Let us assume a very simple dust opacity law, which roughly mimicks the real behavior of dust opacities: the model of Ivezic

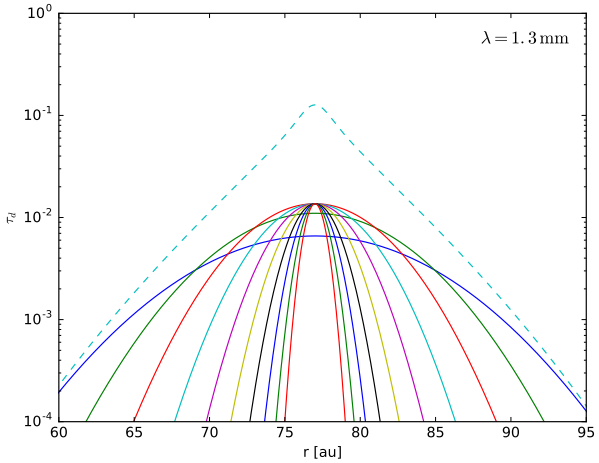

Fig. 4. As Fig. 3, but now the vertical optical depth at $\lambda = 1.3\,\mathrm{mm}$ (ALMA band 6) is shown. The opacity model of Ivezic et al. (1997) was used to compute these from the size distribution.

et al. (1997), where we take the scattering opacity zero for simplicity. In this simple but illustrative opacity model the cross section of a grain with radius a is the geometric cross section πa^2 for $2\pi a > \lambda$ (with λ the wavelength), while it is reduced by a factor $(2\pi a/\lambda)$ for $2\pi a < \lambda$. This means that for $2\pi a > \lambda$ the opacity (that is, the cross section per unit mass) is $\kappa = 3/4\xi_{\rm dust}a$ where $\xi_{\rm dust}$ is the material density, here taken to be $\xi_{\rm dust} = 2\,\mathrm{g/cm^3}$. For $2\pi a < \lambda$ this is reduced by a factor $(2\pi a/\lambda)$ and thus becomes independent of a.

It can be seen from Fig. 4 that at the peak of the trap all grain sizes contribute equally to the optical depth. That is because, with our opacity model, the larger grains (the ones with $2\pi a > \lambda$) have an opacity equal to their geometric cross section per unit dust mass, which goes as $1/a$. The smallest grains (the ones with $a = 0.01$ and $a = 0.167$) have $2\pi a < \lambda$, which means that their opacity remains constant with a. Hence, for these two curves in Fig. 4 the contribution to the peak optical depth drops below those of the other grains. Of course, with a more realistic opacity model this can change somewhat, but the rough principle remains valid.

More important is to notice that the relative contributions of the grain sizes to the peak optical depth may change if a different grain size distribution is chosen. Here we chose the MRN size distribution ($q = 1/2$), but that was a rather arbitrary choice. Given the complexity of the dust growth processes in protoplanetary disks, it is not at all said that the MRN distribution should be considered a preferred one. The reader may experiment with other values of q or entirely different grain size distribution shapes altogether.

3.4. Effect of the degree of trapping on the appearance of the ring

With this simple analytic dust trapping model we can investigate how the degree of trapping affects the appearance of the dust ring. For a model with a single grain size this is easy to predict: if the turbulence is weak enough that the gaussian profile of $\Sigma_{\rm d}(r)$ is narrower than the ALMA beam, then we observe a gaussian profile with the width of the beam. Even if the dust in this narrow ring would be optically thick, the observed ring would have sub-Planckian brightness due to beam-dilution. For stronger turbulence, $\Sigma_{\rm d}(r)$ is spread out wider, and we observe a gaussian profile with the width of the dust profile itself. As in the case of the strongly trapped dust, also the wide rust ring has a Gaussian profile, except that if it is optically thick, the observed profile is flattened at the top due to saturation to the Planck function.

The situation gets more complex if we have a grain size distribution. For a given turbulence strength $\alpha_{\rm turb}$ some grains may be concentrated into a ring that is narrower than the ALMA beam, while others may be more spread out. The strongly concentrated grain population produces a cusp in the brightness, which will be partly smeared out by the beam convolution, while the weakly concentrated grain population produces a broad underlying brightness bump.

To see how this looks in practice we set up a realization of our analytic model. The peak of the pressure is put at $r_0 = 77\,\mathrm{au}$ (corresponding to the inner of the two main rings of AS 209), and the width is chosen to be $w = 30\,\mathrm{au}$ (corresponding to a FWHM of 70 au). Given that the ALMA beam in band 6 has a FWHM of about 35 milliarcseconds, corresponding to 4.4 au for the distance to AS 209, the gas bump is much wider than the beam. The two main dust rings of AS 209 are about 3 beams wide, so that for our wide gas bump model the dust is strongly concentrated. This requires a low turbulent $\alpha_{\rm turb}$ or large grains. As in Section 3.3 we choose a grain size distribution between $a_{\rm min} = 10^{-2}\,\mathrm{cm}$ and $a_{\rm min} = 1\,\mathrm{cm}$, following the usual MRN powerlaw of $q = 1/2$ and a total dust mass of $M = 1.3 \times 10^{-5}\,M_\odot$. The dust material density is taken to be $\xi_{\rm dust} = 2\,\mathrm{g/cm^3}$. We sample this size distribution with 10 grain sizes, evenly distributed in $\ln(a)$. For the disk temperature we choose a simple powerlaw $T(r) = 200\,(r/\mathrm{au})^{-1/2}$. The stellar mass is $M_* = 0.9\,M_\odot$, and the source distance is taken to be $d = 126\,\mathrm{pc}$. All these setting are taken to represent the inner of the two main high-contrast rings of the source AS 209. We set $\mathrm{Sc} = 1$.

The results for several values of $\alpha_{\rm turb}$ are shown in Fig. 5. In the top panel, representing weak turbulence, most of the dust is trapped into a ring more narrow than the beam. A clear cusp can be seen in the un-convolved brightness profile, which is due to the strongly trapped large grains of the size distribution. However, the convolution washes out this cusp for the most part. This situation is equivalent to the simple case of a single dust species being trapped to a narrow unresolved ring. The only dif-

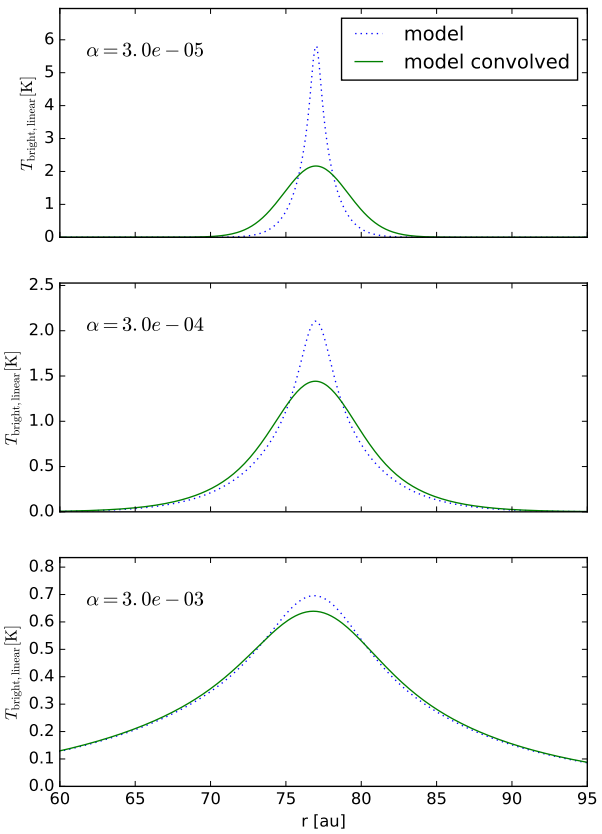

Fig. 5. Results of the analytic dust trapping model for various turbulent strengths, for an MRN powerlaw grain size distribution between $a = 0.01\,$cm and $a = 1\,$cm. The gas pressure bump has a FWHM of 70 au and a peak at $r = 77\,$au. Shown here is the predicted brightness temperature at a wavelength $\lambda = 1.3\,$mm before (dashed) and after (solid) convolution with the ALMA beam, assuming a source distance of $d = 126\,$pc. For a description of the model setup and model parameters, see Section 3.4.

ference is that for a single dust size the ring is either optically thick or optically thin, while in the multi-size case this can be a mix. That does not make a difference for the observed brightness profile, which is a Gaussian either way.

For the case of the strongest turbulence, the bottom panel in Fig. 5, the cusp is still seen in the un-convolved profile, but now the convolution does not wash it out completely. The resulting convolved brightness profile is clearly non-Gaussian as a result. It has a quasi-Gaussian cusp with broad wings. When seen with ALMA such a cuspy profile (narrow at the peak, broad in the wings) should be recognizable.

These findings show that if the turbulent strength is weak, the predicted dust ring width equals the ALMA beam width, and the brightness shape should have the shape of the beam profile (here assumed to be Gaussian). For stronger turbulence, the dust ring becomes indeed broader than the ALMA beam, but then the shape of the observed brightness profile may teach us something about the grain size distribution. Roughly speaking, if the largest grains of the size distribution still get trapped in a narrow ring, this shows up as a cusp in the brightness profile. If the smallest grains of the grain size distribution are too small, the predicted brightness profile would be too broad compared to the observed ring width. In other words: if the observed brightness profile of a observed ring in given source is clearly radially resolved, and if it has a Gaussian shape, then the most likely fit to our analytic model is that of a narrow size distribution (quasi a single grain size) with the right turbulent strength to fit the observed ring width. A broader size distribution, with the appropriately chosen turbulent strength, would yield a cuspy profile, not a Gaussian one.

The two high-contrast rings of AS 209 both appear to fit a Gaussian profile with 2.5 times the width of the ALMA beam (Fig. **??**). In both cases it is therefore likely, according to this analysis, that the dust that is trapped in these rings has a narrow size distribution instead of a broad MRN powerlaw distribution.

3.5. Spectral slope variations across the ring

3.6. Model degeneracies

When trying to infer the effectiveness of dust trapping within the rings with the analytic model of Section 3.2, one notices that there are degeneracies in the possible combinations of parameters. Most obvious is the degeneracy between grain size and turbulence: smaller grains and stronger turbulence may yield the same dust trapping width. But also the width of the gas pressure bump can be compensated: a narrower bump but stronger turbulence (or smaller grains) will yield the same ring width.

[CONTINUE THIS; SOME DEGENERACIES FOLLOW DIRECTLY FROM THE EQUATIONS.]

3.7. Model fits to the ALMA data

We now apply this model to the isolated rings in our ALMA sample (Section 2). Given the degeneracies of the model in many of the parameters, we perform the fitting procedure in three parameters, while fixing the others to a particular choice of values.

[CONTINUE THIS; SHOW THE FIT FIGURES; SHOW THE MCMC CORNER PLOTS]

3.7.1. Could the rings be optically thick at the center?

All rings in our sample show sub-Planckian brightness, at least for the disk temperature assumed in our model. We have calculated the disk midplane temperature using

a simple "flaring angle recipe". If the disks are, however, substantially colder (by up to a factor of 2.5 to 3) then the peak flux of the rings might be consistent with saturated emission, i.e. emission expected from an optically thick disk. So the question is: how sure are we that the rings are sub-Planckian?

To reduce the midplane temperature by a factor of 2 the irradiation flux must be reduced roughly by a factor of $2^4 = 16$. Within the flaring angle recipe this would lead to unrealistically low flaring angle. Presently we assumed $\varphi = 0.02$, so that it would have to reduce to $\varphi = 0.0013$, which is so low that we can no longer trust the flaring angle recipe. However, maybe the outer disk lies in the shadow of the inner disk. To see whether this can reduce the temperature to low enough values, we perform a proper radiative transfer calculation. The results are shown in Appendix (**XXXX**). It shows that **XXXXX**.

There is another issue, however. If the emission saturates to the optically thick brightness, i.e. to the Planck function, then the radial profile of the ring should be flat-topped. This is clearly not what we see in the rings in our sample, with the possible exception of the ring of GW Lup which shows a very slight hint of that. In general, however, it seems that the simple picture of collecting so much dust into the ring that the ring becomes optically thick does not seem to explain the observed radial brightness profiles. On the other hand, optical thickness can also occur on smaller scales, as we will discuss in Section 4.

[TO BE DONE: So far the CMB or cloud background is not included in the model. This has to be improved, because we are working at temperatures close to the CMB. It might reduce the sub-Planckianness, I guess.]

[Question to the experts: The CMB and/or cloud background is automatically filtered out of the interferometric observations, I presume?]

4. Streaming instability, clumping, and the spectral index

Whenever the dust trapping becomes so effective that the volume density of the dust at the midplane of the disk exceeds the gas volume density, the streaming instability may set in (Youdin & Goodman 2005). This produces turbulence and leads to clumping (Johansen & Youdin 2007; Lyra et al. 2008; Bai & Stone 2010). If conditions are right, some of these clumps may gravitationally collapse and form planetesimals (Johansen et al. 2007; Simon et al. 2017; Schäfer et al. 2017). It is believed that this mechanism is the trigger that starts the process of the formation of planets (see Johansen et al. 2014, for a review). If one could find observational evidence of this dust clumping occurring in protoplanetary disks, this would be a major step forward for our understanding of planet formation.

The clumps that are formed in simulations of the streaming instability are, however, typically substantially smaller than a pressure scale height of the disk (Johansen & Youdin 2007; Kowalik et al. 2013). This makes it very hard to spatially resolve these structures, even with ALMA at its highest resolution.

It might, however, be possible to find indications of particle clumping in an indirect way, if it leads to the formation of optically thick clouds of particles surrounded by optically thin regions. Even if we cannot spatially resolve these clouds, the spatially averaged thermal emission from such a clumpy medium has a different spectral slope than that of a homogeneous distribution of dust. If all the dust is concentrated in a multitude of small and very optically thick clumps, then the brightness of this unresolved clumpy medium would be the Planck function times the covering fraction C of the clumps:

$$I_\nu^{\rm obs} = B_\nu(T_{\rm disk})\, C \tag{13}$$

where the limit $C \to 0$ means concentrating all the dust in infinitely dense clumps so that the covering fraction is zero, and $C \to 1$ means having so many clumps that they multiply overlap, when seen in projection from above. In contrast, if all this dust is homogeneously distributed, then the brightness is

$$I_\nu^{\rm obs} = B_\nu(T_{\rm disk})\,(1 - e^{-\tau_\nu}) \tag{14}$$

with τ_ν being the vertical optical depth of the dust in the disk. Reality will likely lie in between these two extreme scenarios, with optically thin dust interdispersed between optically thick clouds.

There are at least two ways by which one could use Eqs. (13, 14) to search for hints of clumpiness. The most direct way is to make use of the different dependencies of these two equations on wavelength $\lambda = c/\nu$. In the case of the clumpy medium with perfectly optically thick clumps (Eq. 13) the brightness follows the Planck curve, whereas for the homogeneous medium (Eq. 14), if it is optically thin (i.e. $1 - e^{-\tau_\nu} \simeq \tau_\nu$), it follows the Planck curve times the opacity law. If we are in the Rayleigh-Jeans domain of the Planck curve, then these two limits are usually referred to as spectral slope $\alpha_{\rm spec} = 2$ and $\alpha_{\rm spec} = 2+\beta$, respectively, where β is defined by $\kappa_\nu \propto \nu^\beta$. At ALMA band 6, for the low temperatures we expect in these disks at large radii, we are no longer strictly in the Rayleigh-Jeans domain, so the spectral slope analysis becomes temperature-dependent, which complicates matters a bit, but the principle remains the same. If the streaming instability is operating in the rings of our sources, and if the numbers work out (see below), then we expect to see $\alpha_{\rm spec} \simeq 2$ within the rings, and $\alpha_{\rm spec} > 2$ between the rings.

There is an important caveat to this idea: the grain size and the corresponding opacity slope may mimick the same spectral signatures as the clumping. This is, in fact, the same degeneracy of the interpretation of the millimeter spectral slope as usual (e.g. Testi et al. 2003), just on a much smaller spatial scale: a scale that remains unresolved even by ALMA. Nevertheless it is worthwhile to investigate if we can find clues that point to clumpiness.

In the scope of this paper we will only do a very simple analysis: we will verify if, under the most benign conditions, the above mentioned optically thick/thin clumpy medium is at all possible. This is not granted, because these rings are several tens of au large, and therefore it requires a lot of mass to make dust clumps optically thick at 1.3 millimeter wavelength. Furthermore, these dust clouds cannot have a density in excess of the Roche density, because then they would immediately gravitationally collapse. Therefore, we cannot make the clumps arbitrary dense and compact.

So let us construct the most optimistic model of a dust cloud. The highest possible density of a cloud is the Roche density, defined by

$$\rho_{\rm Roche}(r) = \frac{9}{4\pi}\frac{M_*}{r^3} \tag{15}$$

where M_* is the stellar mass and r is the distance to the star. We take $\rho_{\rm cloud} = \rho_{\rm Roche}$. The simplest opacity model for a dust grain is that of Ivezic et al. (1997), where we omit the scattering part:

$$\kappa(a) = \frac{3}{4}\frac{1}{\xi\, a}\begin{cases} 1 & \text{for } \lambda < 2\pi a \\ 2\pi a/\lambda & \text{for } \lambda > 2\pi a \end{cases} \tag{16}$$

where a is the grain radius and ξ is the material density of the dust grain ($\xi = 3.6$ for amorphous olivine, $\xi = 2.0$ for silica **CHECK**). For a given wavelength λ (in our case $\lambda = 0.13\,$cm for ALMA band 6), the most optimistic opacity is therefore $\kappa = (3\pi/2)/\xi\lambda$, for all $a \le \lambda/2\pi$. For ALMA band 6 and $\xi = 2\,{\rm g/cm^3}$ this is $\kappa = 18.1\,{\rm cm^2/g}$. The largest grain size to still have this opacity is therefore $a = \lambda/2\pi$, which for ALMA band 6 is $a = 0.02\,$cm. We make a spherical cloud of this dust with radius R. The optical depth through the cloud center is then

$$\tau = 2R\rho_{\rm cloud}\kappa \tag{17}$$

To obtain the effect of an optically thick/thin clumpy medium, these clouds have to be sufficiently optically thick, not just marginally. So let us demand a minimal optical depth of $\tau = 4$. This gives a minimal cloud radius of

$$R \gtrsim \frac{2}{\rho_{\rm Roche}\kappa} = 0.11\frac{1}{\rho_{\rm Roche}} = 0.15\frac{r^3}{M_*} \tag{18}$$

in CGS units (for ALMA band 6). Note that this scales linearly with $\rho_{\rm cloud}/\rho_{\rm Roche}$, so that if we choose a much less "critical" cloud density of, say, $\rho_{\rm cloud} = 0.1\,\rho_{\rm Roche}$, then the cloud should become $10\times$ larger and $100\times$ more massive.

If we want these clouds to be part of an unresolved clumpy medium, they should be substantially smaller than the pressure scale height of the disk, and substantially smaller than the ALMA band 6 resolution. Let us take the example of the source AS 209, with $M_* = 0.9\,M_\odot$, and its two high-contrast rings at 74 au and 120 au, respectively. This gives minimal cloud radii of $R \gtrsim 4\times10^{-3}\,$au and $R \gtrsim 22\times10^{-3}\,$au, respectively. Clouds of size similar to these minimal values are indeed much smaller than the beam width, and are therefore unresolved. This does not mean that there cannot be any smaller clumps/clouds. It only means that any smaller clouds would be optically thin, and we would thus not see any effect of these clumps on the unresolved brightness: these clouds would have a spectral slope equal to that of an optically thin non-clumpy model. At any rate, this estimate shows that, at least in principle, it is possible that the rings we see in our data consist, in fact, of numerous unresolved optically thick clouds interdispersed with optically thin dust (or without any dust in between). Given that such an unresolved, but optically thick, set of clumps has a lower spectral slope $\alpha_{\rm spec}$ than an optically thin dusty medium, an analysis of the measured spectral slope variations over the radial profile of the rings *may* give us some clues as to whether clumpiness occurs or not in these rings, even if we cannot resolve the clumps themselves. We would expect that within the ring the spectral slope is closer to $\alpha_{\rm spec} \simeq 2$ (modulo deviations from Rayleigh-Jeans) than in the inter-ring region.

However, the grain size segregation mechanism, that larger grains are more concentrated in the ring than smaller grains, also tends to produce this signature. This is particularly the case if the big grains (which are closest to the ring peak) are larger than $\lambda/2\pi$ while the small grains are smaller than $\lambda/2\pi$. To distinguish between the roles of size seggregation and clumping, we need an independent way to probe the grain size. Perhaps the effects of self-scattering induced polarization (**?**) may provide such an avenue.

Even if we can distinguish between size-sorting and clumping, we still have to clarify whether the required total dust mass for the clumping scenario is reasonable, and whether the required 'filling factor' is consistent with simulations of the streaming instability. Both questions are related. Let us go back to the two prominent isolated rings of AS 209. The peak linear brightness temperature is 3.5 K for the inner one and 2.7 K for the outer one. In our model the disk midplane temperature is 13 K for the inner and 10 K for the outer ring, which translates (for $\lambda = 0.13\,$cm) into a linear brightness temperature of 8 K and 5.6 K, respectively. If the disk were optically thick, we would thus expect to observe a linear brightness temperature of 8 K and 5.6 K, which are only about 2 times higher.

[TODO: Handle the CMB and cloud background, which might reduce the sub-Planckianness we observe.]

This means that the filling factor of these clouds, as projected vertically toward the observer, must be quite high, of the order of 50%. **[At this point we can calculate the minimum mass in dust needed for this]**

In principle the disk could be warmer than we assume, leading to a larger saturation brightness, and thus a lower required filling factor. But given that a $2\times$ higher disk temperature requires a $16\times$ higher irradiation flux, we expect at most a factor of 2 uncertainty in the required filling factor.

Checking whether this filling factor is consistent with the expectation of simulations of the streaming instability is not easy. Such data are not published for the models describing the streaming instability so far. We can only do a "by eye" check of the figures in those papers (**give a few example papers here**). Such an exercise gives us the impression that the typical fraction of the simulation box that is covered by the dense cluster regions, as projected vertically, is typically substantially less than 50%. If this impression is true, then the ring emission seen in our sample cannot be explained by a set of spatially unresolved optically thick clouds. That does not imply, however, that the streaming instability does not operate in these rings. It only implies that if it does, it will be hidden below an optically thick shroud of more extended dust.

4.1. Under which conditions should the streaming instability set in?

While in Section 4 we investigated if we can recognize the ongoing streaming instability in our data if it is taking place in the disk, in this Section we will compute, with our analytic dust trapping model, under which condition we would *expect* that the streaming instability will operate in the first place. This depends on the total dust mass locked in the trap, the grain sizes and the turbulent strength. To make analytic estimates it is easiest to assume a single grain size, instead of a grain size distribution.

FINISH THIS SECTION

5. Discussion

5.1. Gap depth estimates from 2-D hydrodynamic simulations

Dong & Fung (2017) presented a systematic study of the gap opening profiles for given planetary masses, and analyzed the rings seen in scattered light of 5 sources (HD 97048, TW Hydra, HD 169142, LkCa15 and RX J1615).

5.2. Condition for the streaming instability

In the literature it is often mentioned that the streaming instability requires a dust-to-gas surface density ratio of $\Sigma_{\rm d}/\Sigma_{\rm g} \gtrsim 0.02$ or higher to operate **XXXXXXXX**. This can, however, not be directly compared to our models, because this value of 0.02 was found for models without any pre-determined turbulence. The turbulence in those models was induced by the streaming instability itself or, if the streaming instability does not operate, by the Kelvin-Helmholtz instability (**XXXX**). In the analytic model of this Section, on the other hand, we set the turbulence strength by hand, by setting $\alpha_{\rm turb}$ to some value. In essence, we assume that there is another source of turbulence, such as the magnetorotational instability (**XXXX**) or the vertical shear instability (**XXXX**), that determines the mixing of the dust in the disk.

According to Youdin & Goodman (2005) the true criterion for the onset of the streaming instability is the ratio of dust and gas *volume* densities $\rho_{\rm d}/\rho_{\rm g} \gtrsim 1$. For a given surface density ratio $\Sigma_{\rm d}/\Sigma_{\rm g}$, the midplane volume density ratio, for a single grain species with midplane Stokes number ${\rm St} \ll 1$, depends on the turbulent strength as

$$\frac{\rho_{\rm d}}{\rho_{\rm g}} \simeq \left(1 + \frac{\rm St}{\alpha_{\rm turb}}\right) \frac{\Sigma_{\rm d}}{\Sigma_{\rm g}} \tag{19}$$

The criterion of $\Sigma_{\rm d}/\Sigma_{\rm g} \gtrsim 0.02$ mentioned in the literature thus relates to the criterion $\rho_{\rm d}/\rho_{\rm g} \gtrsim 1$ via the turbulent strength and the Stokes number. Given that we do not compute the turbulent strength but prescribe it, we should rely on the more fundamental volume density criterion of Youdin & Goodman (2005) to assess whether the dust in our model triggers the streaming instability or not.

In our analytic setup of Section 3.4, the dust ring is about 5 times narrower than the gas bump. Assuming that initially the dust-to-gas ratio was 0.01, this implies a dust-to-gas surface density ratio at the peak of the ring of 0.05, which is in excess of the usual 0.02 value. But as long as ${\rm St} \lesssim 19\alpha_{\rm turb}$, Eq. (19) shows that the midplane volume density ratio still stays below unity and no streaming instability sets in.

5.3. Dust trapping in the horseshoe region and in resonances

The 1-D approach of the DISKLAB models make it impossible to treat the trapping of particles in the horseshoe region. The low-α models of **Liu et al. 2018** show that this may be a significant effect. However, this tends to produce non-axisymmetric rings: there will clearly be a dearth of dust near the location of the planet, and a slight enhancement of dust near the L4 and L5 Lagrange points. Given that the rings we see so far in the multi-ringed protoplanetary disks are angularly symmetric, this appears to be ruled out. That means that the 1-D approach is justified, but we do have to ensure that we are not in the regime where such non-axisymmetric horseshoe-trapping is important. Generally the horseshoe region tends to gradually deplete over time, but the time scale depends on the turbulent viscosity, with low-α disks depleting slower.

Another issue is the potential for large particles to get trapped in a resonance of a planet instead of in a classical dust trap **REFERENCE; the Dong double-gap is different, though**. This requires high Stokes number, generally ${\rm St} \gg 1$ (**is this true?**). Given that grain growth models tend to keep grains below this limit (**see e.g. Birnstiel et al.**), this is less likely to play a role.

5.4. Multiple gaps with a single planet

Dong, Li & Li (2017) and **Bae, Zhu & Hartmann (2017)** show that for very low-α disks a planet can open multiple gaps in the disk rather than just a single one. The contrast of these rings and gaps in the gas can be large

(factor of 2; see Bae et al.), and thus clearly constitute dust traps. Dong et al. show that these gaps can even be observable for very low mass planets.

[**TODO: We can do a simple model of dust trapping for their case.**]

Fung & Chiang (2017) have shown that low mass planets in nearly inviscid disks can avoid migration and can be responsible for disk accretion in spite of the low viscosity.

5.5. Interpretation of the millimeter flux in terms of grain size

A common rule of thumb for interpreting millimeter and sub-millimeter fluxes and intensities from thermal dust emission is that you "observe the grain size equal to the wavelength you observe at". This rule is based on the tendency of the dust opacity derived from a Mie calculation to peak at wavelength around $\lambda \sim 2\pi a$, with a the grain radius. For $\lambda \ll 2\pi a$ the opacity becomes nearly constant while $\lambda \gg 2\pi a$ it drops. This effect is even stronger for the scattering opacity. The validity of this rule of thumb relies, however, on the grain size distribution itself. For the simple **Ivezic et al. (1997)** opacity law, it is only valid for grain size distribution powerlaws obeying **XXXXXXXXXXX**. [**TODO: Maybe here do an experiment with full opacity laws.**]

Acknowledgements. The authors acknowledge support by the High Performance and Cloud Computing Group at the Zentrum für Datenverarbeitung of the University of Tübingen, the state of Baden-Württemberg through bwHPC and the German Research Foundation (DFG) through grant no INST 37/935-1 FUGG. This research was initiated at the "Stars, Planets and Galaxies" meeting at the Harnackhaus in Berlin, April 2018. Part of this work was also funded by the DFG Forschergruppe FOR 2634 "Planet Formation Witnesses and Probes: Transition Disks".

References

ALMA Partnership, Brogan, C. L., Pérez, L. M., et al. 2015, ApJL, 808, L3
Andrews, S. M., Wilner, D. J., Hughes, A. M., Qi, C., & Dullemond, C. P. 2009, ApJ, 700, 1502
Andrews, S. M., Wilner, D. J., Zhu, Z., et al. 2016, ApJL, 820, L40
Bai, X.-N. & Stone, J. M. 2010, ApJ, 722, 1437
Barge, P. & Sommeria, J. 1995, A&A, 295, L1
Benisty, M., Stolker, T., Pohl, A., et al. 2017, A&A, 597, A42
Birnstiel, T., Dullemond, C. P., & Brauer, F. 2010, A&A, 513, A79
Brauer, F., Dullemond, C. P., Johansen, A., et al. 2007, A&A, 469, 1169
Casassus, S., van der Plas, G., M, S. P., et al. 2013, Nature, 493, 191
Cieza, L. A., Casassus, S., Pérez, S., et al. 2017, ApJL, 851, L23
Dong, R., Zhu, Z., Fung, J., et al. 2016, ApJL, 816, L12
Dubrulle, B., Morfill, G., & Sterzik, M. 1995, Icarus, 114, 237
Fedele, D., Carney, M., Hogerheijde, M. R., et al. 2017, A&A, 600, A72
Fedele, D., Tazzari, M., Booth, R., et al. 2018, A&A, 610, A24
Güttler, C., Blum, J., Zsom, A., Ormel, C. W., & Dullemond, C. P. 2010, A&A, 513, A56
Huang, J., Andrews, S. M., Cleeves, L. I., et al. 2018, ApJ, 852, 122
Isella, A., Guidi, G., Testi, L., et al. 2016, Physical Review Letters, 117, 251101
Ivezic, Z., Groenewegen, M. A. T., Men'shchikov, A., & Szczerba, R. 1997, MNRAS, 291, 121
Johansen, A., Blum, J., Tanaka, H., et al. 2014, Protostars and Planets VI, 547
Johansen, A., Oishi, J. S., Mac Low, M.-M., et al. 2007, Nature, 448, 1022
Johansen, A. & Youdin, A. 2007, ApJ, 662, 627
Klahr, H. H. & Henning, T. 1997, Icarus, 128, 213
Kowalik, K., Hanasz, M., Wóltański, D., & Gawryszczak, A. 2013, MNRAS, 434, 1460
Kretke, K. A. & Lin, D. N. C. 2007, ApJL, 664, L55
Lyra, W., Johansen, A., Klahr, H., & Piskunov, N. 2008, A&A, 479, 883
Marino, S., Perez, S., & Casassus, S. 2015, ApJL, 798, L44
Pinilla, P., Benisty, M., & Birnstiel, T. 2012a, A&A, 545, A81
Pinilla, P., Birnstiel, T., Ricci, L., et al. 2012b, A&A, 538, A114
Powell, D., Murray-Clay, R., & Schlichting, H. E. 2017, ApJ, 840, 93
Schäfer, U., Yang, C.-C., & Johansen, A. 2017, A&A, 597, A69
Simon, J. B., Armitage, P. J., Youdin, A. N., & Li, R. 2017, ApJL, 847, L12
Testi, L., Natta, A., Shepherd, D. S., & Wilner, D. J. 2003, A&A, 403, 323
van der Marel, N., van Dishoeck, E. F., Bruderer, S., et al. 2013, Science, 340, 1199
Whipple, F. L. 1972, in From Plasma to Planet, ed. A. Elvius, 211
Youdin, A. N. & Goodman, J. 2005, ApJ, 620, 459
Youdin, A. N. & Lithwick, Y. 2007, Icarus, 192, 588
Zsom, A., Ormel, C. W., Güttler, C., Blum, J., & Dullemond, C. P. 2010, A&A, 513, A57